Improving the Back Surface Field on an Amorphous Silicon Carbide Thin Film Photocathode for Solar Water Splitting

Perez-Rodriguez, Paula; Cardenas-Morcoso, Drialys; Digdaya, Ibadillah A.; Raventos, Andrea Mangel; Procel, Paul; Isabella, Olindo; Gimenez, Sixto; Zeman, Miro; Smith, Wilson A.; Smets, Arno H.M.

DOI
10.1002/cssc.201800782

Publication date
2018

Document Version
Accepted author manuscript

Published in
ChemSusChem

Citation (APA)
Perez-Rodriguez, P., Cardenas-Morcoso, D., Digdaya, I. A., Raventos, A. M., Procel, P., Isabella, O., Gimenez, S., Zeman, M., Smith, W. A., & Smets, A. H. M. (2018). Improving the Back Surface Field on an Amorphous Silicon Carbide Thin Film Photocathode for Solar Water Splitting. *ChemSusChem*, *11*(11), 1797-1804. https://doi.org/10.1002/cssc.201800782

CHEMISTRY & SUSTAINABILITY

CHEMSUSCHEM

ENERGY & MATERIALS

Accepted Article

Title: Improving the back surface field on an amorphous silicon carbide (a-SiC:H) thin film photocathode for solar water splitting

Authors: Paula Perez-Rodriguez, Drialys Cardenas-Morcoso, Ibadillah A. Digdaya, Andrea Mangel Raventos, Paul Procel, Olindo Isabella, Sixto Gimenez, Miro Zeman, Wilson A. Smith, and Arno H.M. Smets

To be cited as: *ChemSusChem* 10.1002/cssc.201800782

Link to VoR: http://dx.doi.org/10.1002/cssc.201800782

A Journal of

ChemPubSoc Europe

WILEY-VCH

www.chemsuschem.org

Improving the back surface field on an amorphous silicon carbide (a-SiC:H) thin film photocathode for solar water splitting

Paula Perez-Rodriguez*[a], Drialys Cardenas-Morcoso[b], Ibadillah A. Digdaya[c], Andrea Mangel Raventos[a], Paul Procel[a], Olindo Isabella[a], Sixto Gimenez[b]**, Miro Zeman[a], Wilson A. Smith[c], Arno H.M. Smets[a]

Abstract: Amorphous silicon carbide (a-SiC:H) is a promising material for photoelectrochemical (PEC) water splitting due to its relatively small bandgap energy and high chemical and optoelectrical stability. This work studies the interplay between charge carrier separation and collection, and their injection into the electrolyte, when modifying the semiconductor/electrolyte interface. By introducing an n-doped nanocrystaline silicon oxide (nc-SiO_x:H) layer into a p/i amorphous silicon carbide (a-SiC:H) photocathode, the photovoltage and photocurrent of the device can be significantly improved, reaching values higher than 0.8 V. This results from enhancing the internal electric field of the photocathode, reducing the Shockley-Read-Hall (SRH) recombination at the crucial interfaces due to better charge carrier separation. In addition, the charge carrier injection into the electrolyte is enhanced by introducing a TiO_2 protective layer due to better band alignment at the interface. Finally, the photocurrent was further enhanced by tuning the absorber layer thickness, arriving at a thickness of 150 nm, after which the current saturates to 10 mA cm^{-2} at 0 V vs. RHE in a KPH electrolyte at pH 4.

Introduction

The growing world energy demand and the depletion of fossil fuels require alternatives to the current energy system. Solar energy offers a cleaner and more sustainable alternative due to the high amount of solar energy availability and relatively easy installation and maintenance of solar systems. However, due to daily and seasonal fluctuations in irradiance, energy storage plays an important role in the implementation of solar energy. Daily irradiance variations can be tackled by using batteries, but seasonal variations need alternative storage methods that offer a cheaper and more energy dense solution [1]. Hydrogen is a plausible option to tackle this problem, since it can be easily stored in tanks or further converted into other hydrocarbons by using carbon dioxide (CO_2), which have a high energy density and low cost. Moreover, the resulting products can be stored for long periods of time with minimum losses such as self-discharge [2]. Direct hydrogen production using solar driven water splitting has attracted considerable attention in the last years [3] [4] [5] [6] [7]. In particular, photoelectrochemical (PEC) devices provide a simple and elegant solution to hydrogen production using solar energy.

Photoelectrochemical production of hydrogen from water splitting is based on a material which absorbs light and generates electron-hole pairs. These charge carriers are then separated within the semiconductor and used to drive the two half-reactions at the cathode and anode, which produce highly pure hydrogen and oxygen on the electrode surfaces, respectively. There are several characteristics that a semiconductor needs to fulfil for its use in a PEC device: adequate optical properties, good charge separation, chemical stability, and correct band alignment with respect to the potentials of the water splitting reaction [7]. In addition, the materials used need to be earth-abundant in order to achieve a cost-effective solution. The PEC field has dedicated extensive effort to the search for a suitable material to drive the water splitting reaction. Among the thin-film semiconductors based on metal oxides tested for this application are TiO_2 [8], [9] [10], Fe_2O_3 [11] [12], WO_3 [13] or $BiVO_4$ [14]. These semiconductors can produce relatively high photovoltages, due to their relatively large bandgap energy. However, they absorb only a small fraction of the solar spectrum. Therefore, there has recently been a shift to investigate non metal-oxide photolectrodes with smaller bandgap energies, such as silicon, which in theory could enhance the amount of photocurrent generation [15] [16] [17]. Zhu et al. [18] proposed an amorphous silicon carbide (a-SiC:H) photocathode with a bandgap energy of 2.0 eV. Moreover, Han et al. [19] introduced a gradient boron doped homojunction to improve the internal electric field and charge carrier collection. Thus, the attention has recently started to shift from material science towards device architecture design, using strategies such as the inclusion of different doped layers [3] [19] [20] and the introduction of a surface field at the semiconductor/electrolyte interface for a more selective charge carrier collection [21]. These results show that not only the material used as photoelectrode is important, but also the charge carrier separation and collection. Therefore, the optimization of internal electric fields can play an important role on the performance of PEC devices [22]. However, the introduction of an internal electric field also modifies the interface energies between the semiconductor and the device, which might be detrimental to the charge carrier injection into the electrolyte. Thus, two main limiting factors to consider when designing the device architecture of a photoelectrode can be defined: the charge carrier separation and the charge carrier injection into the electrolyte. This paper aims at studying the principles behind the charge carrier separation, collection and injection of a photocathode when modifying the semiconductor/electrolyte interface.

In order to improve the charge carrier collection, the different electronic junctions formed in the device must be optimized [23]. If the interface contains many defects, Shockley-Read-Hall (SRH) recombination, also called defect-assisted charge carrier recombination, can occur at the junction. Homojunctions such as the (p)a-SiC:H/(i)a-SiC:H previously introduced lead to limited SRH recombination due to the reduced amount of defects such as dangling bonds or lattice mismatch at the interface. That is not the case with some other junctions like heterojunctions, semiconductor/metal or semiconductor/electrolyte junctions, where the differences between the material lattice, possible dangling bonds, voids and other defects can lead to higher levels of SRH recombination at the interface. To avoid this effect, an electric field and selective contacts can be introduced near the surface to screen away the minority charge carriers. This concept has already been successfully used for semiconductor/metal contacts in the photovoltaic (PV) field [24] [25].

[a] Photovoltaic Materials and Devices (PVMD) group, Delft University of Technology. Delft, The Netherlands
[b] Institute of Advanced Materials (INAM), Universitat Jaume I,12006, Castelló de la Plana, Spain
[c] Materials for Energy Storage and Conversion (MECS), Department of Chemical Engineering, Delft University of Technology. Delft, The Netherlands

Corresponding authors:
* p.perezrodriguez@tudelft.nl
** sjulia@fca.uji.es

The present study focuses on the improvement of an a-SiC:H photocathode by using the concepts developed in the PV field such as passivation of interfaces, selective contacts and electric fields by optimizing a back surface field. In addition, the chemical reaction at the interface must be considered, and the band alignment between the energy levels of the reaction and the semiconductor bandgap energies must be considered. Here, the know-how of the PV field regarding the enhancement of the internal electric field and charge carrier collection is combined with the PEC expertise on the solar water splitting reaction and charge carrier injection to develop a more efficient PEC device. To improve the overall performance of a-SiC:H photocathode, the effect of introducing a back surface field by adding an n-doped nanocrystalline silicon oxide (nc-SiO_x:H) layer to create a p/i/n structure was studied. The characteristics of nc-SiO_x:H can be tuned depending on the oxygen content [26], and therefore it is widely used as an n-layer for thin film silicon solar cells. This layer enhances the electric field created inside the semiconductor, which facilitates the charge carrier separation. In addition, it serves as a selective contact to improve charge carrier collection, and to passivate surface defects that can lead to SRH recombination. Furthermore, when an undoped TiO_2 protective layer is introduced at the semiconductor/electrolyte interface, both the band alignment and chemical stability can be improved [27] [28]. The general structure of the a-SiC:H photocathode with both the (n)nc-SiO_x:H and the TiO_2 layer is shown in Figure 1.

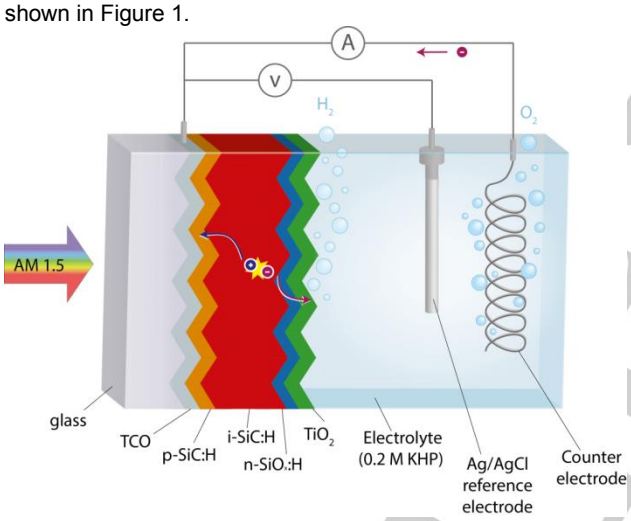

Figure 1. Schematic representation of the photoelectrochemical measurements carried out in a three-electrode configuration.

Results and Discussion

Including an n-layer on an amorphous silicon carbide (a-SiC:H) photocathode is expected to improve its performance due to a better charge carrier separation and collection, and a reduction in the SRH recombination. Previously, protective layers such as TiO_2 have demonstrated not only to improve stability, but also to create a back surface field, improving the carrier injection at the semiconductor/electrolyte interface [29]. However, TiO_2 has a relatively high density of states and a relatively high lattice mismatch with a-SiC:H [27]. This causes recombination at the a-SiC:H/TiO_2 interface, and therefore limits the photoelectrode efficiency. In addition, the created electric field strength is low, since TiO_2 has a relatively low donor density. Alternatively, a phosphorous doped nanocrystalline silicon oxide ((n)nc-SiO_x:H) could be included in this structure. Phosphorous doped nanocrystalline silicon oxide, (n)nc-SiO_x:H, is often used in thin film silicon solar cells as an n-layer to improve the internal electric field and charge carrier selectivity, in addition to its favourable optical properties [26, 30]. Thus, it is expected to improve the performance of the a-SiC:H photocathode.

Figure 2 shows the photoelectrochemical behaviour of different a-SiC:H photocathodes with and without a (n)nc-SiO_x:H layer and with and without a TiO_2 layer. These results show that the introduction of a back surface field, either by introducing an (n)nc-SiO_x:H or a naturally n-type TiO_2 layer, largely improves the onset potential of the photocathode from approximately -0.4 V vs. RHE to about 0.6-0.7 V vs. RHE. The photocathode with only the (n)nc-SiO_x:H layer has a slightly higher onset potential, but the one with only TiO_2 presents a steeper JV slope, indicating a lower series resistance, which suggests that the injection of charge carriers into the electrolyte is facilitated. This might be due to a better band alignment of the TiO_2, which would reduce the resistance at the TiO_2/electrolyte interface. Finally, by combining both layers, the performance of the photocathode is further improved, resulting in onset potentials higher than 0.8 V vs. RHE, a steep slope indicating lower series resistances, and a current density of 10 mA/cm^2 at 0 V vs. RHE. This current density is comparable to other state-of-the-art devices, with current densities ranging between 8-12 mA/cm^2 for a-SiC:H photocathodes. This paper focuses on analysing the fundamental semiconductor physics associated with these high performances. First, the limiting mechanisms (charge carrier separation or injection) in each case are discussed, and then further optimizations are presented.

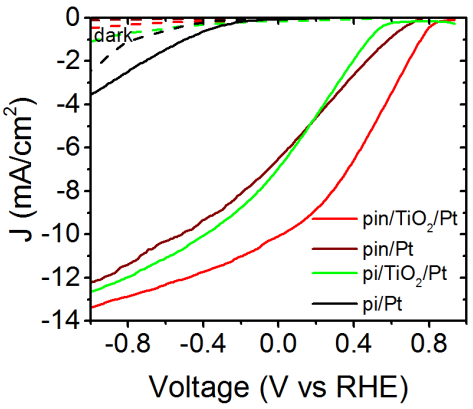

Figure 2. JV characteristics as a PEC device for the different samples with and without an n-layer, and with and without TiO_2 in a three-electrode configuration.

Analysis of the Limiting Mechanisms

The main two limiting mechanisms in these devices are considered to be the charge carrier separation and collection, and the charge carrier injection into the electrolyte. The effects observed in Figure 2 have been associated with these two mechanisms. In order to confirm the effect of the band alignment and reduced series resistance of the (n)nc-SiO_x:H and the TiO_2 layer with the electrolyte, an EIS study at a range of frequencies (10^{-1}-10^5 Hz) has been performed to identity the most suitable frequency to carry out a single frequency Mott-Schottky analysis. In this analysis, the capacitance is the depletion layer capacitance. Figure 3 shows the Mott-Schottky plots of the two

materials in order to compare the band alignment effects of a (n)nc-SiO_x:H and a TiO_2 layer in contact with the electrolyte. [29]

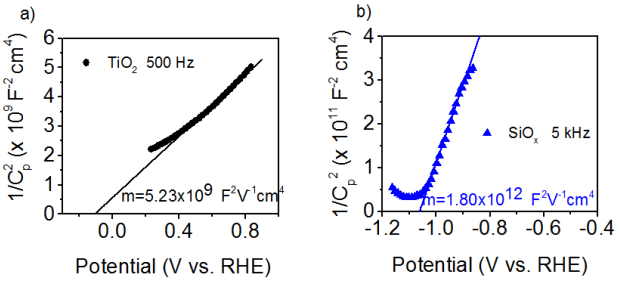

Figure 3. Mott-Schottky plots of a) a 100 nm TiO_2 layer, and b) a (n)nc-SiO_x:H layer with thickness of 100 nm. The variable m indicates the slope of the fitted linear function

From the dark EIS measurements, the flat band potential of (n)nc-SiO_x:H, V_{fb}, can be calculated by using the relation [31]

$$\frac{1}{C^2} = \frac{2}{e\varepsilon_0\varepsilon_r N_D}\left(V - V_{fb} - \frac{kT}{e}\right) \quad (1)$$

where C represents capacitance, e is the elementary charge, ε_0 is the permittivity in vacuum, ε_r is the relative permittivity of the (n)nc-SiO_x:H, k is the Boltzmann constant and T is the temperature, taken as 298 K.
The flatband potential can be calculated from the intercept of the Mott-Schottky plot with the voltage-axis displayed in Figure 3, as

$$intercept\ voltage\ axis = V_{fb} + \frac{k_B T}{e} \quad (2)$$

The obtained flatband potential estimates are -0.13 V vs. RHE for the TiO_2 sample of 100 nm, and -1.06 V vs. RHE for the case of 100 nm (n)nc-SiO_x:H samples. These values were used in further simulations of the different band diagrams in Sentaurus software, shown in Figure 4. These simulations estimate the energy band diagram structure of an entire structure based on the individual film properties.
Since the donor density of (n)nc-SiO_x:H is expected to be larger compared to TiO_2 due to the intentional doping introduced, the band alignment of (n)nc-SiO_x:H with the electrolyte is less optimal. This has been confirmed by determining the activation energy of the layers, which represents the difference between the conduction band and the Fermi energy level. The activation energy was determined by dark conductivity measurements of the isolated layers at different temperatures. An activation energy of 66.03 meV was measured for (n)nc-SiO_x:H, and 266.36 meV for TiO_2. This is also an input to the electrical simulations presented in Figure 4 to better determine the band alignment of the different layers. The higher flat band potential of (n)nc-SiO_x:H suggests a higher band bending at the semiconductor/electrolyte interface, creating the energy barrier shown in Figure 4d, leading to charge recombination at the semiconductor/electrolyte interface. On the other hand, TiO_2 has a better alignment with the energy level of the reaction in the solution, where the flatband potential is close to zero. This could explain the differences observed between the p/i/n/Pt and the p/i/TiO_2/Pt photocathodes. It must also be noted that the (n)nc-SiO_x:H samples were not stable in the solution, creating uncertainties in the measurement. It is thus possible that the flatband potentials of this material are even more negative, highlighting the benefits of adding a TiO_2 layer on the surface. On the other hand, (n)nc-SiO_x:H improves the internal electric field and charge carrier collection selectivity. If TiO_2 is used at the surface of the (n)nc-SiO_x:H samples, the energy barrier at the interface with the electrolyte is slightly reduced, as shown in Figure 4f, facilitating charge injection and reducing recombination. The p/i/n/TiO_2/Pt system outperforms the p/i/TiO_2/Pt structure due to the effects on the interface between (i)a-SiC:H and TiO_2, where the selectivity and electric field produced is not as strong as with the (n)nc-SiO_x:H. Another factor that these simulations show is the creation of a small energy barrier at the (n)nc-SiO_x:H/TiO_2 interface due to the work function of these different layers. However, the disadvantage of this interface is overcome by the advantages of an improved internal electric field and band alignment.

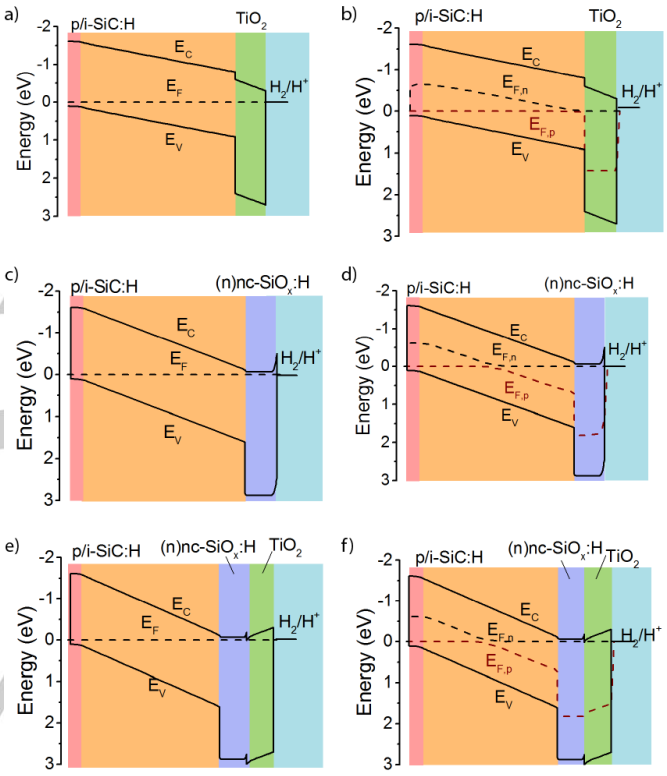

Figure 4. Simulations of the band alignment of the photocathode with respect to the solution with a p/i/n junction including a,b) TiO_2, c,d) nc-SiO_x:H and e,f)the combination of both in the dark (a,c,e) and illuminated under one sun (b,d,f)

To deconvolute the surface effects of this combination of layers, an EIS analysis was performed for the (n)nc-SiO_x:H and (n)nc-SiO_x:H/TiO_2 samples, shown in Figure 5. By fitting the resulting data to the Randles' equivalent circuit, resistances and capacitances at the semiconductor/electrolyte interface could be obtained. It can be seen that the resistance at the interface is higher for the case of the (n)nc-SiO_x:H/TiO_2 combination both in dark and illuminated conditions. This is probably caused by the additional resistances included by the TiO_2 layer. This was confirmed by measuring the lateral conductivity of the layer at 25 °C, which resulted in a value of 0.304 S/cm for the (n)nc-SiOx:H and 6.60 10^{-5} S/cm for the TiO_2. Nevertheless, the reduction of the resistance upon illumination is higher when TiO_2 is included due to a better charge carrier injection from the SiOx:H layer into the electrolyte. Regarding the capacitance, both the (n)nc-SiO_x:H sample and (n)nc-SiO_x:H/TiO_2

combination show a fairly constant capacitance with voltage, and an increase when illuminated with respect to dark conditions. This suggests the that the double layer capacitance dominates the capacitive response of the electrode in both cases. The overall capacitance is however higher in the (n)nc-SiO_x:H sample, which could stem from photocorrosion, limited in the other sample due to the protection provided by TiO_2.

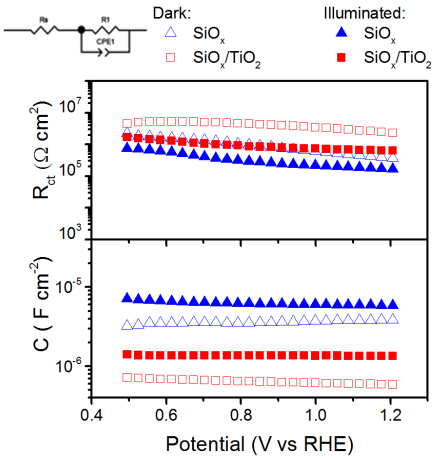

Figure 5. EIS analysis of a 100nm (n)nc-SiOx:H and a 100 nm (n)nc-SiOx:H /20 nm TiO_2 film in dark conditions and under AM1.5 illumination (0.5M KHP pH4), together with the equivalent Randles' circuit including a Warburg element. Note that these measurements have been done for positive potentials, and thus under reverse bias.

To explore if these trends can be extrapolated to the whole device, the same measurements were performed on p/i/n a-SiC:H samples, with and without a TiO_2 layer, as shown in Figure 6. The impedance spectroscopy measurements carried out for this analysis did only show a single arc. This means that a single process is dominating the response of the system, although there are different processes taking place, which are invisible for impedance spectroscopy, probably because they appear at a time scale not sensitive for our experimental technique. We assigned the resistance to the charge transfer process, since it is extremely high to account for any other internal process in the multi-layered structure. Additionally, the constant evolution of the capacitance versus applied voltage is also an indication of a double layer dielectric capacitance, so it is reasonable to associate the elements of the Randles' circuit to the double layer capacitance and charge transfer resistance. The presence of a Warburg element in the equivalent circuit of Figure 6 accounts for the diffusion of electrolyte species, (see Supplementary Information, Figure SI1).The resistance shows less variation between dark and illuminated conditions compared to the results in Figure 5. The inclusion of the TiO_2 layer in this case results in a lower resistance, probably due to the better band alignment and easier charge carrier injection. Regarding the capacitance, it increases with illumination in both cases, especially in the case of the sample with a TiO_2 layer. However, it must be noted that these capacitances have been reduced by at least one order of magnitude as compared to the individual layers, indicating the benefit of having a p/i/n structure for charge carrier transfer at the interface.

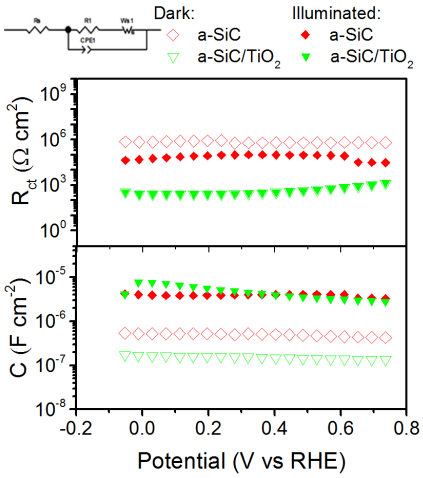

Figure 6. EIS analysis of a-SiC:H and a-SiC:H/TiO_2 samples in dark and under AM1.5 illumination conditions (0.5M KHP pH4), together with the equivalent Randles' circuit including a Warburg element, which accounts for the diffusion of electrolyte species. Note that these measurements have been done for positive potentials, and thus under reverse bias.

In summary, the introduction of a TiO_2 layer improves the band alignment of the photocathode, and therefore the charge carrier injection into the electrolyte. Regarding the introduction of a (n)nc-SiO_x:H layer between the absorber material and the TiO_2, it seems to achieve a lower defect density, lower SRH recombination, higher charge carrier selectivity and higher internal electric field. By combining these two layers, a more efficient photocathode can be achieved.

Photocathode Optimization and Stability

In order to further study and optimize the effects of the improvement of charge carrier separation and collection in the semiconductor device, and the extraction of charge carriers at the semiconductor/electrolyte interface, the two considerations were decoupled. First, the semiconductor internal electric field and optical absorption were studied by isolating the semiconductor device as a PV solar cell, where the charge carrier extraction is assumed not to be the limiting factor (Figure 7a, b). Second, to look at the effects of the catalyst and electrolyte, the electrochemical characteristics were measured (Figure 7c). The improvements in the internal electric field when introducing a (n)nc-SiO_x:H layer in the p/i structure were confirmed for different n-layer thicknesses, as can be seen in Figure 7a and Table 1. The n-layer thickness can change the optical performance of the photoelectrode, as well as affecting possible tunnelling effects through this layer. Moreover, if the layer is too thin, pinholes might appear creating short-circuit paths. When no n-layer is present, the open circuit voltage when measured as a solid-state PV junction is less than 0.4 V. When a layer as thin as 10 nm is introduced, the open circuit voltage and short circuit current are drastically improved, reaching almost the same values as thicker layers. However, the fill factor in this case is very poor, probably due to inhomogeneities in the layer thickness that may cause areas without n-layer within the cell and possible tunnelling effects. A thickness of 20 nm for the n-layer appears to be large enough for a good performance, reaching an open circuit voltage of 0.8 V and short circuit current density of more than 10 mA/cm^2, with a fill factor of almost 0.6. Further increase of the n-layer thickness leads to a slight increase in the fill factor and short circuit current that could be

related to the optical properties of nc-SiO_x, which enhance the back reflection. [30, 32] Figure 7b shows that when no n-layer is included, a big fraction of the light with wavelengths higher than 450 nm is not absorbed. The introduction of an n-layer as thin as 10 nm already improves these results. The optimum appears to be 30 nm, especially due to a higher current density. However, this improvement is not so apparent in the PEC measurements in Figure 7c, where the differences of the saturation current densities are within measurement error. This difference could be caused by the absence of Ag back reflector when measuring PEC JV characteristics. In addition, it seems that the (n)nc-SiO_x:H thickness is not the limiting factor of the photocathode performance, as long as it is present. This can be seen in the onset potential in Figure 7c, where virtually no difference can be seen. Therefore, by ensuring that the semiconductor internal electric field effectively separates and collects the charge carriers, it is clear that the charge carrier injection into the electrolyte is the limiting factor of these devices. Finally, it is interesting to compare these onset-potentials (0.78-0.81 V) with the open circuit voltages of the solid-state measurements (0.81-0.83 V) when the thickness has reached the thickness of 20 nm. There seems to be a negligible difference of around 20-30 mV between these two measurements, which can be related to the dependence of the overpotentials on the charge carrier injection into the electrolyte and the catalytic effects at the semiconductor/electrolyte interface.

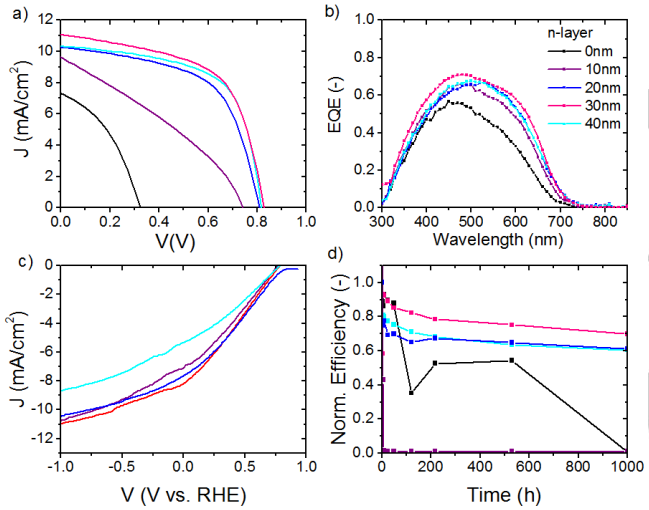

Figure 7. a) Solid state JV curves, b) EQE measurements, c) PEC JV curves and d) light-induced degradation 1000 h of the a-SiC:H photocathodes at different n-layer thicknesses including a TiO_2 protective layer and a Pt catalyst.

Table 1. External parameters of the solid state JV characteristics with different n-layer thickness

n-layer thickness (nm)	V_{OC} (V)	J_{SC} (mA/cm^2)	FF	Efficiency (%)
0	0.32	7.25	0.41	0.94
10	0.74	9.53	0.33	2.35
20	0.81	10.25	0.59	4.82
30	0.83	11.05	0.59	5.36
40	0.82	10.32	0.62	5.26

These results suggest that once the layer has reached the critical thickness of 20 nm, the properties cannot be improved much further by increasing the n-layer thickness. Moreover, the PEC characteristics of the 40 nm sample suggest that if the thickness of the n-layer is increased too much, the charge carriers might not be able to be easily injected into the electrolyte due to the additional resistances, and might prevent possible tunnelling of charge carriers to occur.

When performing the light induced degradation experiments shown in Figure 7d, an additional advantage of this n-layer was found. The performance of the cells measured as solid-state devices degraded up to efficiencies of almost 0 % in 1000 h of exposure for the samples with thinner n-layer. On the other hand, samples with thicker n-layer have an efficiency change in the order of 30-40 % with respect to the initial value. This suggests that the a-SiC:H absorber layer without an n-layer tends to degrade upon illumination. This could be explained by the mechanism of the Staebler-Wronski effect. [33] When charge carriers are generated in the absorber material but cannot be separated, they will recombine. Upon recombination, energy is released within the absorber material, creating the metastable defects that cause light induced degradation. By introducing efficient means of separating the charge carriers and reducing the recombination inside the absorber material, this effect can be reduced. Thus, the introduction of an n-type nc-SiO_x:H improves the optical and electrical characteristics of the photoelectrode, as well as enhancing its stability upon illumination at ambient conditions. Note that the results regarding 0 and 10 nm are not consistent with this trend. This is due possible deposition and measurement irregularities. However, the lower performance with respect to the samples with 20 nm or over have consistently measured for shorter stretches of time. Since increasing the thickness of the n-layer further than 20 nm does not have a big effect on the optical or electrical properties of the photocathode, this thickness has been chosen as the standard for further studies.

To further improve the photocathode, also the light absorption in the absorber layer must be taken into account. Thus, to increase the light absorption in the p/i/n a-SiC:H photocathode, the i-layer thickness can be optimized. Figure 8 shows an increase in short circuit current density with thicker i-layer due to the higher light absorption. Figure 8a indicates that if the i-layer thickness is as small as 50 nm, extra resistances and possible pinholes may appear, causing shunts and a very poor fill factor. For thicker layers this is not a problem anymore, since the i-layer is then thick enough to maintain a higher homogeneity. This effect is also reflected in the fill factor shown in Table 2. Regarding the optical effects, the photocathodes with i-layers thicker than 150 nm show a saturation of the current density, display only a slight improvement in absorption in the red part of the spectrum (Figure 8b). However, the solid-state JV measurement shows a lower fill factor for 200 nm than for 150 nm. Thus, the additional absorption would be compensated by the enhanced recombination due to extra defects introduced, creating a balance between the optical and electrical properties of the layer. It is also apparent from the EQE measurements in Figure 8b that the EQE in the short wavelength region reduces with an increase of i-layer thickness. This can be explained by the reduced charge carrier collection at the p-layer, since the electric field is weakened.

When looking at the PEC performance, the trend again seems to saturate at 150 nm. In this case, the series resistance for both 150 nm and 200 nm is the same, indicating that the series resistance in the solution is probably the limiting effect. Since there is not much difference between 150 nm and 200 nm, 150 nm was chosen as the optimum layer thickness for this device as it would suffer less from light induced degradation [33]. Chronoamperometry measurements were performed on the p/i/n/TiO_2 photocathode with an i-layer thickness of 150 nm to determine its stability in the electrolyte, displayed in Figure 8d. These measurements show that the photocathode can be reasonably stable for more than an hour, with a reduction of the

photocurrent of less than 20%. When only considering the solid state degradation upon illumination, the photocathode with 20 nm n-layer showed a reduction in the short circuit current of about 10%. Thus, it could be assumed that about half of the stability loss is related to the Staebler-Wronski effect, while the other half would be caused by chemical degradation. Although the detailed study of the chemical degradation observed was out of the scope of this paper, literature suggests that it might be related to catalyst detachment. [22] Therefore, it seems that, at least in the first hour, the solid state stability and chemical stability are comparable.

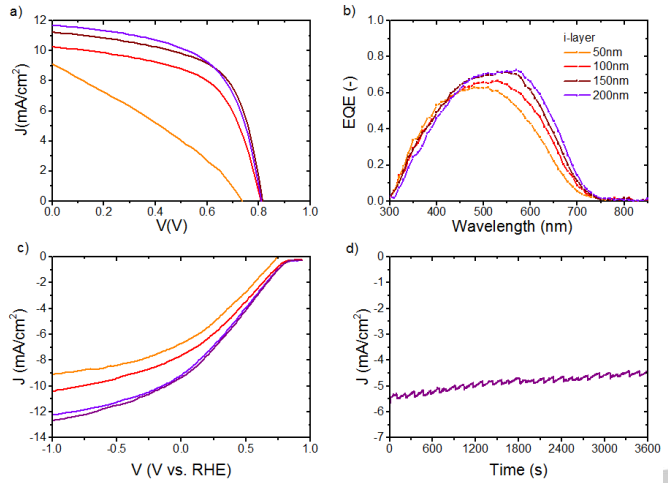

Figure 8. a) Solid state JV curves, b) EQE measurements and c) PEC JV curves of the a-SiC:H photocathodes at different i-layer thicknesses with a TiO_2 protective layer and Pt catalyst, and d) stability test for the 150 nm a-SiC:H photocathode with an applied voltage of 0 V vs. RHE

Table 2. External parameters of the solid state JV characteristics with different i-layer thickness

i-layer thickness (nm)	V_{OC} (V)	J_{SC} (mA/cm^2)	FF (-)	Efficiency (%)
50	0.74	9.02	0.32	2.09
100	0.81	10.25	0.59	4.82
150	0.82	11.21	0.60	5.58
200	0.81	11.68	0.59	5.57

Conclusions

This paper demonstrates the importance of device design to enhance the separation and collection of charge carriers, and reduce the recombination losses, not only for PV but also for the PEC field. By introducing an n-doped nanocrystaline silicon oxide (nc-SiO_x:H) layer onto an amorphous silicon carbide (a-SiC:H) photocathode, its performance for solar water splitting can be improved. It can highly enhance the internal electric field and charge carrier selectivity of the photocathode, improving the charge carrier separation and collection. In addition, it also protects the photocathode of degradation upon illumination by reducing the SRH recombination. However, to improve the band alignment with the electrolyte, a TiO_2 layer is needed. The minimum thickness of the n-SiO_x:H layer was determined to be 20 nm. To enhance light absorption without affecting the charge collection performance, the optimum absorber a-SiC:H layer thickness of this p/i/n photocathode was found to be 150 nm. Using these specifications, an onset potential of 0.8 V vs RHE and a current density of 10 mA/cm^2 at 0 V vs. RHE can be achieved, with a loss in efficiency of only 20% after 1 h of operation.

Experimental Section

Photocathode deposition. The a-SiC:H and nc-SiO_x:H layers were deposited using Radio Frequency Plasma Enhanced Chemical Vapour Deposition (RF-PECVD). Asahi UV-type, consisting of a textured glass with an FTO coating, was used as a substrate. A p/i or p/i/n structure was used, in which the p-type layer was a 10 nm film of boron doped hydrogenated silicon carbide ((p)a-SiC:H), the i-type layer was a film of intrinsic hydrogenated amorphous silicon carbide ((i)a-SiC:H), and the n-type layer was phosphorous doped nanocrystalline silicon oxide ((n)nc-SiO_x:H). Unless otherwise stated, the i-type layer was 100 nm and the n-type layer was 20 nm. The precursor gases used were SiH_4, CH_4, H_2 and CO_2. Doping of p and n layers was realized using the gases B_2H_6 and PH_3, respectively. Different layers (p, i, n) were deposited in different chambers of an Elettrorava cluster PECVD tool to avoid cross contamination. As a front contact, a 300 nm Al stripe was deposited on the FTO by electron beam evaporation in a Provac evaporator, and then a silver wire was attached to it using carbon paste.
For some of the PEC measurements, a titanium oxide (TiO_2) layer of 20 nm was deposited using an in-house Atomic Layer Deposition (ALD) system located at TU Delft. During deposition, the substrate temperature was 200 °C. Tetrakis (dimethylamino)-titanium (TDMAT) and water were used as precursors for the Ti and O, respectively. The growth rate was 0.6-0.8 Å per cycle, measured by ellipsometry. The samples were further annealed at 300 °C for an hour to crystallize the material. Subsequently, a layer of 1 nm Pt catalyst was deposited using sputtering with radio frequency (RF) in a PREVAC sputtering tool, with a deposition rate of 0.5-0.6 Å/s. This relatively high deposition rate allows the formation of nanostructures, which improve its catalytic activity. [34]

Solid-state characterization techniques. The activation energy of the different layers was determined by measuring the dark conductivity of the layer at different temperatures between 60 and 135 °C, and fitting the results to an Arrhenius plot.
The external quantum efficiency (EQE) represents the percentage of incident photons on the device that produce charge carriers that would be collected. Here, the EQE was measured with an in-house system in the PVMD group, TU Delft, consisting of a Xe lamp attached to a monochromator. A Ge calibration diode was used for correcting the spectrum. When measuring EQE, a back contact of 200 nm Ag, 30 nm Cr and 500 nm Al was deposited by physical evaporation on the photocathode. This stack enhances reflectivity and ensures the chemical stability of the layer. The short circuit current was obtained by integrating the EQE weighted with the AM1.5 solar spectrum.
The solid state measurements of the JV characteristics were done under a double lamp Class AAA Wacom solar simulator. The temperature at Standard Test Conditions (STC) of 25 °C was maintained by a Julaboo cooling system integrated in the measurement stage. When measuring solid-state JV curves, a metal back contact was also deposited, defining a cell area of 0.16 cm^2. The short circuit current density (J_{SC}) obtained from these measurements was normalized by the J_{SC} obtained by integrating the EQE output over the AM1.5 spectrum.
Finally, amorphous silicon (a-Si:H) is known to degrade under illumination due to the Staebler-Wronski effect [33], related to metastable defects inside the material. In order to study if a-SiC:H has a similar behaviour, the a-SiC:H cells with a back contact were exposed to constant illumination of 1 sun at 25°C for 1000 h, and the solid-state JV characteristics of these cells were measured several times during this process. The light-induced degradation is presented as the normalized value of the external parameters with respect to the initial state.

Photoelectrochemical (PEC) characterization techniques. The JV characteristic as a PEC device was measured using an aqueous 0.2 M potassium hydrogen phthalate (Alfa Aesar, 99.99%) solution at pH 4 as electrolyte. The measurements were carried out with a 3 electrode configuration, as shown in Figure 1, with an Ag/AgCl reference electrode (XR300, Radiometer Analytical) and a Pt wire counter electrode. This configuration was chosen to focus on the photocathode performance, independently from the anode behaviour. The solar simulator used was a Newport Sol3A Class AAA. The illumination area in contact with the solution was a 3 mm radius circle, with a total area of 0.283 cm^2. Note that the current densities achieved by this method my vary from the solid-state JV measurements due to differences in the diffused light and inaccuracies on the equipment. The solid-state measurements are considered more reliable when determining current densities, since they have been corrected using the EQE measurements.

To determine the stability in the electrolyte, chronoamperometry measurements were performed, where the current is measured on time at a constant voltage applied. Note that the current density measurements obtained as PEC are less accurate due to internal reflections and diffused light effects within the measurement equipment.
Electrochemical Impedance Spectroscopy (EIS) measurements were performed in the dark on an (n)nc-SiO_x:H layer of 100 nm deposited on a Asahi substrate, and on a 100 nm TiO_2 sample in order to determine the flatband position of the relevant interfaces. EIS measurements were also carried out on the full photocathodes consisting of a-SiC:H and a-SiC:H/TiO_2 structures. A Metrohm Autolab potentiostat was used, with a reported measurement error of ±0.2 %. [35] Impedance data were collected between 10^{-2} - 10^{6} Hz using a 20 mV amplitude voltage perturbation and analysed with the ZView software (Scribner associates). Finally, to better understand the obtained behaviour, electrical simulations were performed using the SENTAURUS software.

Acknowledgements

We thank Rene van Swaaij for his helpful comments and insight during the course of this work. This work is part of the research programme of the Foundation for Fundamental Research on Matter (FOM-13CO19), which is part of the Netherlands Organisation for Scientific Research (NWO).

Keywords: Charge carrier injection • Amorphous silicon carbide • Hydrogen • n-type SiO_x • TiO_2 protective layer

[1] H. Ibrahim, A. Ilinca, J. Perron, *Renewable and Sustainable Energy Reviews* **2008**, *12*, 1221-1250.
[2] G. Nicoletti, N. Arcuri, G. Nicoletti, R. Bruno, *Energy Conversion and Management* **2015**, *89*, 205-213.
[3] F. F. Abdi, L. Han, A. H. M. Smets, M. Zeman, B. Dam, R. v. d. Krol, *Nature communications* **2013**, *4*.
[4] Z. Li, W. Luo, M. Zhang, J. Feng, Z. Zou, *Energy and Environmental Science* **2013**, *6*, 347-370.
[5] B. A. Pinaud, J. D. Benck, L. C. Seitz, A. J. Forman, Z. Chen, T. G. Deutsch, B. D. James, K. N. Baum, G. N. Baum, S. Ardo, H. Wang, E. Miller, T. F. Jaramillo, *Energy and Envirnmental Science* **2013**, *6*, 1983-2002.
[6] F. Urbain, V. Smirnov, J.-P. Becker, A. Lambertz, U. Rau, F. Finger, *Solar Energy Materials and Solar cells* **2015**.
[7] M. G. Walter, E. L. Warren, J. R. McKone, S. W. Boettcher, Q. Mi, E. A. Santori, N. S. Lewis, *Chem. Rev.* **2010**, *110*, 6446-6473.
[8] A. Fujishima, K. Honda, S. Kikuchi, *Journal of Chemical Society Japan* **1969**, *72*, 108-113.
[9] G. K. Mor, K. Shankar, M. Paulose, O. K. Varghese, C. A. Grimes, *Nano Letters* **2005**, *5*, 191-195.
[10] Y. J. Hwang, C. Hahn, B. Liu, P. Yang, *ACS Nano* **2012**, *6*, 5060-5069.
[11] P. S. Bassi, Gurudayal, L. H. Wong, J. Barber, *Phys. Chem. Chem. Phys.* **2014**, *16*, 11834-11842.
[12] H. Dotan, K. Sivula, M. Gratzel, A. Rotschild, S. C. Warren, *Energy and Environmental Science* **2011**, *4*, 958-964.
[13] M. Malizia, B. Seger, I. Chorkendorff, P. C. K. Vesborg, *Journal of Materials Chemistry A* **2014**, *2*, 6847-6853.
[14] F. F. Abdi, N. Firet, R. van de Krol, *Chem Cat Chem* **2013**, *5*, 490-496.
[15] J.-W. Jang, C. Du, Y. Ye, Y. Lin, X. Yao, J. Thorne, E. Liu, G. McMahon, J. Zhhu, A. Javey, J. Guo, D. Wang, *Nature communications* **2015**, *6*, 7447.
[16] J. Oh, T. G. Deutsch, H.-C. Yuan, H. M. Branz, *Energy and Environmental Science* **2011**, *4*, 1690-1694.
[17] L. Shen, C. He, J. Qiu, S.-M. Lee, A. Kalita, S. B. Cronin, M. P. Stoykovich, J. Yoon, *ACS Appl. Mater. Interfaces* **2015**, *7*, 26043-26049.
[18] F. Zhu, J. Hu, I. Matulionis, T. Deutsch, N. Gaillard, A. Kunrath, E. Miller, A. Madan, *Philosophical magazine* **2009**, *89*, 2723-2739.
[19] L. Han, I. A. Digdaya, T. W. F. Buijs, F. F. Abdi, Z. Huang, R. Liu, B. Dam, M. Zeman, W. A. Smith, A. H. M. Smets, *Journal of Materials Chemistry A* **2015**, *3*, 4155-4162.
[20] R. Marschall, *Advanced Functional Materials* **2014**, *24*, 2421-2440.
[21] I. A. Digdaya, L. Han, T. W. F. Buijs, M. Zeman, B. Dam, A. H. M. Smets, W. A. Smith.
[22] I. A. Digdaya, P. Perez-Rodriguez, M. Ma, G. W. P. Adhyaksa, E. C. Garnett, A. H. M. Smets, W. A. Smith, *Journal of Materials Chemistry A* **2016**, *4*, 6842-6852.
[23] I. A. Digdaya, G. W. Adhyaska, B. J. Tzesniewski, E. C. Garnett, W. A. Smith, *Nature Communications* **2017**, *8*, 15968.
[24] J. Mandelkorn, J. J.H. Lamneck, in *Record of 9th Photovoltaic Specialists Conference*, **1972**.
[25] M. Gratzel, *Inorganic Chemistry* **2005**, *44*, 6841-6851.
[26] V. Smirnov, A. Lambertz, B. Grootoonk, R. Carius, F. Finger, *Journal of Non-Crystalline Solids* **2012**, *358*, 1954-1957.
[27] H. H. Pham, L.-W. Wang, *Phys. Chem. Chem. Phys.* **2015**, *17*, 541-550.
[28] A. G. Scheuermann, K. W. Kemp, K. Tang, D. Q. Lu, P. F. Satterthwaite, T. Ito, C. E. D. Chidsey, P. C. McIntyre, *Energy and Environmental Science* **2016**, *9*, 504-516.
[29] I. A. Digdaya, L. Han, T. W. F. Buijs, M. Zeman, B. Dam, A. H. M. Smets, W. A. Smith, *Energy and Environmental Science* **2015**, *8*, 1585-1593.
[30] S.-T. Hwang, D. J. You, S. H. Kim, S. Lee, H.-M. Lee, *Solar Energy Materials and Solar Cells* **2013**, *113*, 79-84.
[31] K. Gelderman, L. Lee, S. W. Donne, *Journal of Chemical Education* **2007**, *84*, 685-688.
[32] V. Demontis, C. Sanna, J. Melskens, R. Santbergen, A. H. M. Smets, A. Damiano, M. Zeman, *Journal of Applied Physics* **2013**, *113*, 064508.
[33] D. L. Staebler, C. R. Wronski, *Applied Physics Letters* **1977**, *31*, 292-294.
[34] E. Slavcheva, I. Radev, G. Topalov, E. Budevski, *Electrochemical Acta* **2007**, *53*, 362-368.
[35] M. Autolab, **2018**.

Entry for the Table of Contents

FULL PAPER

This paper systematically decouples the photovoltaic and catalytic effect for a monolithic device for water splitting for the first time.

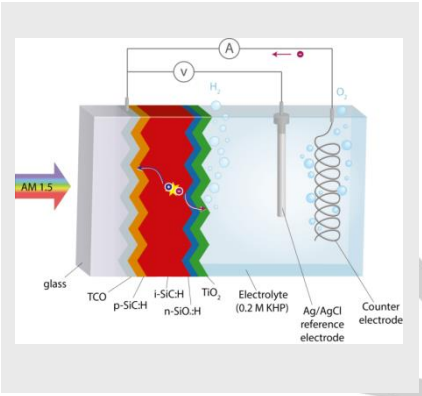

Paula Perez-Rodriguez[a], Drialys Cardenas-Morcoso[b], Ibadillah A. Digdaya[c], Andrea Mangel Raventos[a], Paul Procel[a], Olindo Isabella[a], Sixto Gimenez[b]**, Miro Zeman[a], Wilson A. Smith[c], Arno H.M. Smets[a]

Page No. – Page No.

Improving the back surface field on an amorphous silicon carbide (a-SiC:H) thin film photocathode for solar water splitting